The design and performance of an x-ray micro-focusing system using differentially deposited elliptical mirrors at the National Synchrotron Light Source

J. M. Ablett and C. C. Kao
National Synchrotron Light Source, Brookhaven National Laboratory, Upton, New York 11973

A. Lunt
Spectrogon AZ, Inc., 1683 West Grant Road, Suite 105, Tucson, Arizona 85745

(Received 26 November 2001; accepted for publication 1 July 2002)

The National Synchrotron Light Source X13 straight section houses two insertion devices: a small-gap undulator (IVUN) and an elliptically polarized wiggler. The low vertical β function at the center of the straight section, where IVUN is located, produces an extremely small vertical source size [full width at half maximum (FWHM) = 15.5 μm]. To take advantage of the small source size for a wide range of x-ray microbeam applications, a Kirkpatrick–Baez pair of 10 cm long elliptically figured mirrors, fabricated using a differential-deposition technique, was designed and implemented. A FWHM focused spot size of 3 μm (vertical) by 9 μm (horizontal) was achieved. The performance of this microfocusing system and selected applications are reported. © *2002 American Institute of Physics.* [DOI: 10.1063/1.1505656]

I. INTRODUCTION

Due to the very low vertical β function at the center of the X13 straight section of the National Synchrotron Light Source (NSLS) x-ray storage ring, the vertical electron beam size, proportional to $\sqrt{\beta}$, is only 15.5 μm full width at half maximum (FWHM). To exploit this unique property, a small-gap insertion device development program was initiated at the NSLS almost a decade ago. This effort led to the successful development of a prototype small-gap undulator, which demonstrated that small-gap devices can be operated without adverse effects on the stored electron beam.[1] Subsequently, in collaboration with the Spring-8 facility in Japan, an in-vacuum small gap undulator (IVUN)[1–3] was developed for the NSLS. These in-vacuum small gap devices have now been adopted widely by many medium energy storage rings, such as the NSLS, to provide undulator radiation into the hard x-ray region.

One of the opportunities offered by IVUN at the NSLS is the possibility of producing high intensity submicron focused x-ray beams that can be used for a wide range of applications. Among the various ways of microfocusing x rays, elliptical mirrors in the Kirkpatrick–Baez arrangement[4] have several advantages: First, they can be used in applications where both white beam and monochromatic beam are required. Second, the focal length is fixed and independent of x-ray energy. Third, they produce a clean beam, with high efficiency in higher harmonics rejection, and well-defined intensity profiles.

The elliptical figure for grazing incident x-ray optics has traditionally been attained by dynamical bending of flat tapered surfaces.[5–7] This method has the advantage of a tunable focal length and has achieved very good mirror figures. Recently, a very appealing means of directly forming elliptical profiles has been demonstrated by Ice *et al.*[8] In this technique, spherical silicon substrates are differentially coated with gold to achieve the desired shape. The potential for focusing intense x-ray beams into micron-sized or submicrons spots are achievable by this method as the fabrication process can deliver figure errors (slope errors) of less than 2 μrad, and rms roughnesses of below 3 Å.

In this article, we report the design and performance of an x-ray microfocusing system, using a rhodium-coated Kirkpatrick–Baez pair of elliptically figured mirrors, for beamline X13B at the NSLS. In this design, a relatively long working distance of 23 cm is used to accommodate high-pressure experiments, which emphasizes the need for maintaining highly accurate surface profiles over longer mirror lengths. Section II briefly describes the insertion devices and the X13B beamline. The optical design and implementation, and the characterization of the system are described in Secs. III and IV, respectively. Finally, a few selected examples are reported in Sec. V to demonstrate the capability of the system.

II. INSERTION DEVICES AND THE X13B BEAMLINE

There are two insertion devices in the X13 straight section of the NSLS x-ray storage ring: IVUN[1–3] and the elliptically polarized wiggler (EPW).[9–13] IVUN is located at the center of the straight section, where the electron beam size is only 15.5 μm (FWHM) in the vertical direction, and 1027 μm (FWHM) in the horizontal direction. The EPW, located 0.9 m downstream of IVUN, produces elliptical polarized light with a fast switching capability, up to 100 Hz.[9–13]

Currently, these two insertion devices are the radiation sources for two NSLS beamlines: X13B (a hard x-ray Beamline) and X13A (a soft x-ray beamline).[14] Soft x rays from the EPW are deflected toward the X13A beamline using a

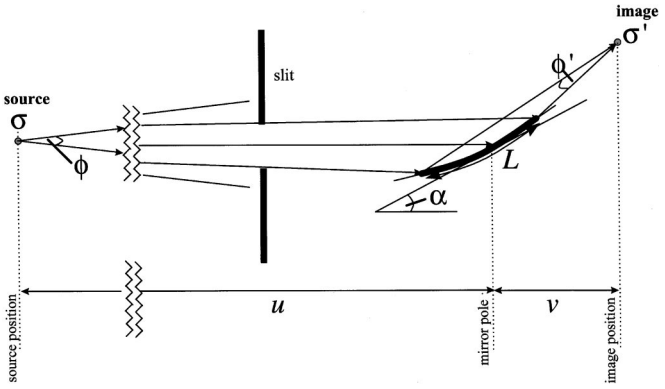

FIG. 1. The geometry of a single microfocusing optic. A slit is placed before the optics to restrict the x-ray beam to the mirror acceptance.

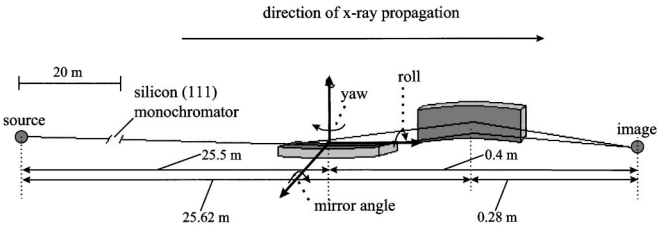

FIG. 2. A schematic of the X13B microprobe Kirkpatrick–Baez arrangement of elliptical mirrors. The rotational degrees of freedom turn about the orthogonal axes that are shown on the vertical focusing mirror. These rotations are needed for accurate positioning of the mirrors into the x-ray beam. The distances from the source to the mirror poles and from the mirror poles to the image location are also labeled.

copper-coated water-cooled spherical mirror. This horizontal deflecting mirror is located ~13 m from the center of the X13 straight section, and takes only half of the horizontal beam from the insertion devices so that both beamlines can be operated simultaneously.

Energy tunability is provided by a water-cooled double-crystal silicon (111) monochromator. To avoid excessive power being applied to the first monochromator crystal, a set of independent water-cooled movable copper slits, positioned 10 m downstream from the center of the X13 straight section, are used to restrict the horizontal and vertical radiation fans. In addition, a retractable graphite filter immediately upstream of the monochromator is used to absorb low energy x rays, and thus further limits the incident power. Together, the slits and filter significantly improve the thermal stability, as well as reducing the thermal distortion of the crystal. This is especially important when performing x-ray spectroscopic measurements utilizing the IVUN device because of the higher power density of this source.

III. OPTICAL DESIGN AND IMPLEMENTATION

In this section, the design and specifications of the X13B microfocusing system will be presented. For the following discussion, it is useful to define terms that will be used to describe the performance of a microfocusing optic. Figure 1 shows a schematic of the layout of a single reflective mirror of length L. The distance from the synchrotron source to the mirror pole is u and the distance from the mirror pole to the focal position is v. At synchrotron radiation facilities, u is typically much longer than v so that the focal length f is given to very good approximation by v. Consideration of the geometrical demagnification and conservation of phase space then lead to the following equations:

$$\frac{v}{u}=\frac{\sigma'}{\sigma}=\frac{\phi}{\phi'}, \tag{1}$$

where σ, σ' are the source and image sizes, and ϕ, ϕ' are the acceptance and convergence angles of the radiation, respectively.

If the central ray from the source makes a grazing angle of incidence α to the mirror surface, then the image distance is given by the focusing properties of a cylinder of radius R

$$v\sim\frac{R\alpha}{2}. \tag{2}$$

It should be noted that with current synchrotron source sizes, microfocusing typically requires demagnifying optics on the order of 100:1 to deliver micron-sized spots, and therefore it is necessary to have relatively short mirrors to minimize the obtainable focal distance. Consequently, the angular source acceptance ϕ for microfocusing optics is usually very limited. Thus, high-brightness undulators are ideally matched to microfocusing optics.

A schematic of the Kirkpatrick–Baez arrangement, as well as relevant distances of the focusing optics at the X13B beamline, are shown in Fig. 2. The rotational degrees of freedom: angle, roll, and yaw, are also denoted. The first mirror focuses the x rays in the vertical direction and the second mirror provides horizontal focusing. The choice of the present configuration is due to a number of considerations: First, the primary objective of the system is to provide focal spot dimensions on the order of microns with the highest possible x-ray flux. Second, for high-pressure experiments, the focal distance has to be long enough to accommodate the diamond-anvil sample cell and a backscattering detector (see Sec. V). Third, the horizontal source size and beam divergence are much larger than those of the vertical.

The basic parameters of the system are then determined by the above considerations and the current technical limit on the size of mirrors that can be differentially coated. Each mirror is 10 cm long, and the distance from the center of the X13 straight-section (IVUN source) to the mirror poles are 25.5 and 25.62 m for the vertical and horizontal focusing mirrors, with focal lengths of 0.4 and 0.28 m, respectively. The lengths of these type of mirrors are the longest manufactured to date and maintaining the figure accuracy over this entire length scale is essential for delivering small x-ray beam and flux to the sample. For zero slope error, a demagnified spot size of $0.24\times11.3\ \mu m^2$ (FWHM) would be obtained. Adding an image blur generated by a 2 μrad figure error in quadrature to the geometrically demagnified image should produce an x-ray microbeam of $3.8\times11.6\ \mu m^2$ (FWHM).

Rhodium was chosen as the deposition metal for forming the elliptical mirrors for high reflectivity throughout the whole energy range of interest: 4–15 keV. In contrast with gold, rhodium is an excellent choice for a microfocusing

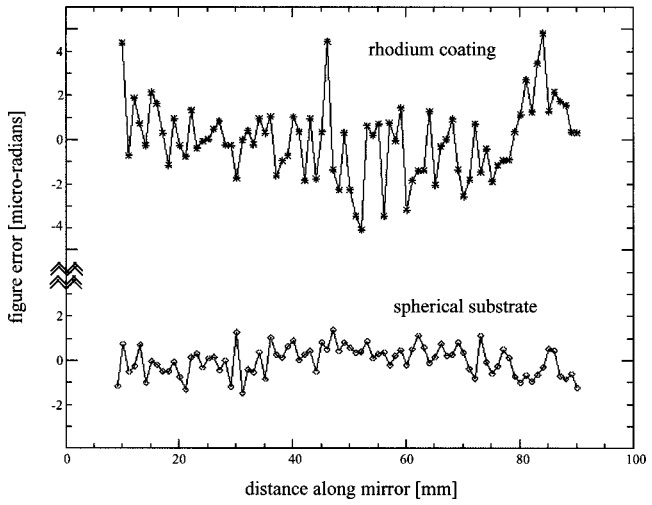

FIG. 3. The residual slope errors of the substrate and deposition profile for the vertical focusing mirror. The rms slope error value for the spherical substrate is only 0.7 μrad. For the elliptical rhodium coating, the rms slope error value is 1.7 μrad.

deposition metal as there are no L edges toward higher x-ray energies which could hinder experimental measurements in this region. The incident angle of both mirrors α was chosen to be 3.8 mrad as a compromise between constraining the maximum energy to below 15 keV and providing a larger source acceptance.

The radii of curvature for the spherical silicon substrates were calculated by fitting a circle to the elliptical profiles that were determined through the SHADOW ray-tracing code,[15] with radii of curvature of 204 and 143 m for the vertical and horizontal mirrors, respectively. The amount of rhodium that needs to be deposited onto the substrates is then the circular fit subtracted from the elliptical curve. The spherical substrates are polished to a very high specification, and it is necessary to measure the profile of the mirror accurately so that any change of the radial parameter can be corrected for in the predetermined deposition profile. A highly accurate substrate profile is essential for maintaining low figure errors once the mirror coating has been deposited. Figure 3 shows both the figure error of the substrate and rhodium coating profile as measured using a LTP II long-trace profiler.[16] For the silicon substrate, the rms figure error is only 0.7 μrad, increasing to 1.7 once the deposition coating has been applied. These data, taken on the vertical focusing mirror, were obtained by subtracting the elliptical slope from the measured slope in the region of ~9–90 mm along the mirror lengths. Due to the manufacturing process, there are some ''roll off'' errors toward the ends of the mirror, which reflect the range of data points in Fig. 3. Similar results were obtained for the horizontal focusing optic.

IV. CHARACTERIZATION OF THE MICROFOCUSING OPTICS

After the mirrors had been fabricated, they were inserted into their respective enclosures and attached to the rotational and translation stages. These were then placed onto a heavy granite table to ensure good vibrational damping. The mirror entrance apertures consisted of rectangular polished tantalum

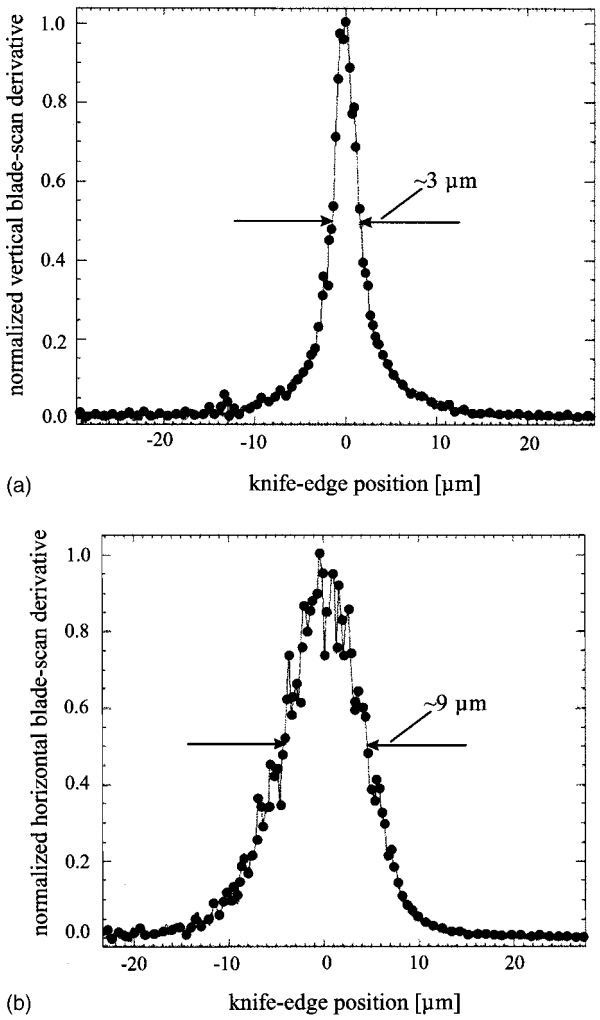

FIG. 4. The derivative of knife-edge scans that were used to determine the x-ray microfocus beam dimensions: (a) vertical direction and (b) horizontal direction.

blocks, which had been prealigned with the x-ray beam. A yttrium-aluminum garnet: Ce scintillator crystal was placed at the predetermined focal position, and the fluorescent light emitted with impinging x rays was viewed on a high-resolution charge coupled device optical microscope. Each mirror was separately aligned and small changes to the mirror angle were performed until the best line focus had been achieved. Both mirrors were then inserted into the x-ray beam to provide both vertical and horizontal focusing.

To measure the focused beam dimensions, a tantalum knife edge, mounted to a submicron computer-controlled sample stage, was scanned across the x-ray beam and the photon flux was monitored using a silicon photodiode placed downstream of the focal position. Small adjustments to the angles of the mirror pair were performed until the best focus had been achieved. The derivative of the flux throughput is shown in Figs. 4(a) and 4(b), and the quality of the microfocusing optics is clearly demonstrated with a FWHM spot size of $\sim 3 \times 9\ \mu m^2$. In the previous discussion, the optics were positioned to use the IVUN source. With the EPW source, a beam size of $\sim 4 \times 10\ \mu m^2$ was obtained.

The ultralow roughness of the mirror material was also verified: With helium flight paths and helium flow through

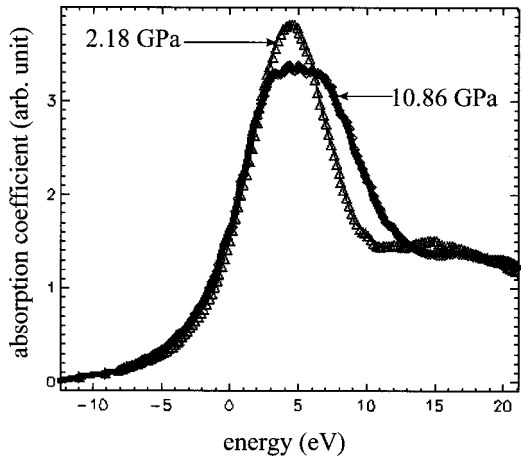

FIG. 5. High-pressure x-ray transmission measurement performed at the rhenium L_3 absorption edge on thallium–rhenium oxide. An abrupt phase transition occurs at ~10 GPa, and this is shown as a large broadening of the white-line feature in this graph. The X13B microfocusing optics were necessary to direct a sufficient number of photons onto the sample which also had to propagate through the diamond anvils located inside the high-pressure sample cell. The energy scale is shown as the difference from the rhenium L_3 edge at 10.535 keV.

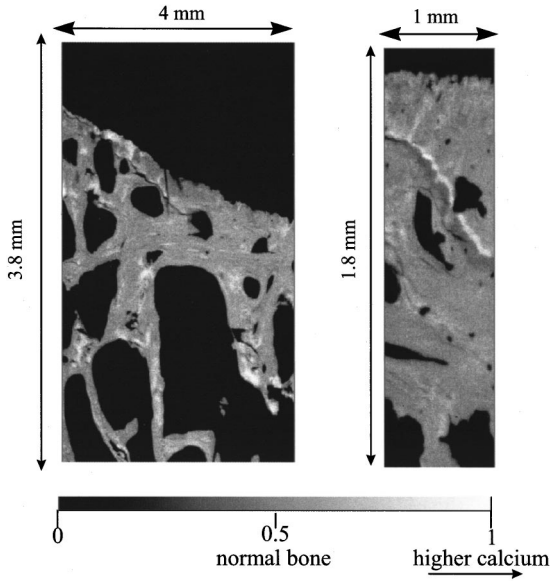

FIG. 6. Calcium fluorescence map taken from an osteoarthritic monkey bone tibia section. The high resolution delivered by the X13B microprobe is clearly visible. There are some interesting areas of high calcium concentration in both maps which are denoted by the lighter shaded areas. The holes within the sections are called osteons and there are also several microcracks.

the mirror chambers, the flux using the IVUN device is 6×10^{10}, 6×10^{9}, and 9×10^{9} photons/s at the first (5.4 keV), second (10.8 keV), and third (16.2 keV), harmonics respectively. Employing the EPW source (with horizontal magnetic field switched off), the flux at energies corresponding to the harmonics of IVUN is 5×10^{9}, 3×10^{9}, and 9×10^{8} photons/s, respectively.

V. SELECTED EXAMPLES

The X13B microfocusing optics were designed to be used for high-pressure research. The long working distance of 23 cm from the end of the horizontal focusing mirror enabled the accommodation of bulky diamond–anvil sample cells such as those of the Mao-Bell type.[17–20]

Thallium–rhenium oxide ($TlReO_4$) was the first material to be studied using the X13B microfocusing optics. This is a particularly interesting material that exhibits an abrupt room-temperature phase transition at ~10 GPa. This transition has previously been investigated using Raman spectroscopy and x-ray diffraction.[21,22] At this pressure, the sample turns from a greyish color to completely black. This striking color change signifies a considerable modification in the band structure of the material.[22] Using the X13B microfocusing optics, an x-ray transmission experiment at the rhenium L_3 absorption edge was conducted to provide further information on this electronic rearrangement. Figure 5 shows the change in the absorption coefficient near the Re L_3 edge. The strong white-line peak that occurs in the vicinity of the edge corresponds to the promotion of electrons from $2p$ to empty $5d$ states. The large broadening of the white-line feature above the pressure-induced phase transition is an important signature of this electronic structural change and could also signify a closing of the band gap.

In high-pressure experiments, it is sometimes not possible to obtain measurements in transmission mode because of sample thickness and incident x-ray energy considerations. However, the long working distance of the X13B microprobe allows for the placing of energy-dispersive detectors in an approximate backscattering geometry. In this layout, self-absorption corrections can be readily applied[23,24] and accurate XANES and extended x-ray absorption fine structure (EXAFS) measurements, from fluorescence x-ray detection, can be determined. High-pressure experiments on praseodymium metal have been conducted using this technique and the data are currently under analysis.

The small x-ray spot size of $\sim3\times9\ \mu m^2$, together with large flux throughput, is well suited to x-ray imaging applications. A preliminary investigation of the calcium distribution within sections of osteoarthritic monkey tibia has recently been conducted in fluorescence mode. This investigation is a unique application of x-ray microbeams and comparison with infrared microspectroscopy,[25] measuring the carbonate/protein and phosphate/protein ratios, is envisaged in the near future. A calcium fluorescence map of osteoarthritic bone is shown in Fig. 6.

VI. DISCUSSION

The design and implementation of differentially coated elliptical x-ray optics have been successfully applied to the construction of the NSLS X13B microfocusing end station. There are many areas of research that can benefit from microfocused x-ray beams. These achromatic optics offer larger collection apertures compared to other microfocusing optics currently available. Differentially deposited mirrors provide an alternative system to traditional bendable optics, and improvements to the fabrication process should further reduce the slope error, and obtain even smaller spot sizes.

The X13B microprobe has enhanced the microfocusing capabilities of the NSLS considerably by providing a focused spot size of ~3 μm in the vertical and ~9 μm in the

horizontal directions at long working distances. Due to the high accuracy of the deposition technique, a large photon flux throughput has been achieved by utilizing almost the full mirror lengths. Submicron focused beams are also possible with this current technology, and will be employed in the near future at the NSLS.

ACKNOWLEDGMENTS

Research carried out at the National Synchrotron Light Source, Brookhaven National Laboratory, which is supported by the U.S. Department of Energy, Division of Materials Sciences and Division of Chemical Sciences, under Contract No. DE-AC02-98CH10886. The authors gratefully acknowledge Dr. P. Her and Dr. L. Assoufid, at the APS metrology facility and Dr. P. Tacaks, at Brookhaven National Laboratory for performing the optical profile measurements. Finally, they would like to thank Dr. G. Ice for many helpful discussions.

[1] P. M. Stefan *et al.*, Nucl. Instrum. Methods Phys. Res. A **412**, 161 (1998).
[2] T. Tanabe *et al.*, Rev. Sci. Instrum. **69**, 18 (1998).
[3] P. M. Stefan, Synchrotron Radiat. News **11**, 22 (1998).
[4] P. Kirkpatrick and A. V. Baez, J. Opt. Soc. Am. **38**, 766 (1948).
[5] H. A. Padmore *et al.*, Synchrotron Radiat. News **10**, 18 (1997).
[6] M. R. Howells *et al.*, Opt. Eng. (Bellingham) **39**, 2748 (2000).
[7] B. X. Yang *et al.*, Rev. Sci. Instrum. **66**, 2278 (1995).
[8] G. E. Ice *et al.*, Rev. Sci. Instrum. **71**, 2635 (2000).
[9] E. Gluskin *et al.*, Brookhaven National Laboratory Report No. BNL-61858, 1995.
[10] A. Friedman *et al.*, Brookhaven National Laboratory Report No. BNL-49175, 1993.
[11] A. Friedman, S. Krinsky, and E. Blum, Brookhaven National Laboratory Report No. BNL-47317 (1992).
[12] S. Krinsky and C. C. Kao, Synchrotron Radiat. News **8**, 38 (1995).
[13] K. J. Randall *et al.*, Brookhaven National Laboratory Report No. BNL-65091, 1998.
[14] Z. Xu *et al.*, Rev. Sci. Instrum. **66**, 1827 (1995).
[15] C. Welnak *et al.*, Rev. Sci. Instrum. **63**, 865 (1992).
[16] P. Z. Takacs *et al.*, Appl. Opt. **38**, 5468 (1999).
[17] H. K. Mao and P. M. Bell, Science **200**, 1145 (1978).
[18] C.-M. Sung, C. Goetze, and H.-K. Mao, Rev. Sci. Instrum. **48**, 1386 (1977).
[19] K. A. Goettel, H. K. Mao, and P. M. Bell, Rev. Sci. Instrum. **56**, 1420 (1985).
[20] H. K. Mao and P. M. Bell, Rev. Sci. Instrum. **50**, 1002 (1979).
[21] L. C. Ming *et al.*, Phys. Rev. B **51**, 12100 (1995).
[22] A. Jayaraman, G. A. Kourouklis, and L. G. VanUitert, Phys. Rev. B **36**, 8547 (1987).
[23] L. Tröger *et al.*, Phys. Rev. B **46**, 3283 (1992).
[24] P. Pfalzer *et al.*, Phys. Rev. B **60**, 9335 (1999).
[25] L. M. Miller *et al.*, Cell Mol. Biol. (Paris) **44**, 117 (1998).